Land subsidence due to natural gas extraction in the Thrace basin (NW Turkey) and its influence on the North Anatolian fault under the Marmara Sea

TOHID NOZADKHALIL

ZİYADİN ÇAKIR

SEMİH ERGİNTAV

UĞUR DOĞAN

THOMAS R. WALTER

Recommended Citation

Land subsidence due to natural gas extraction in the Thrace basin (NW Turkey) and its influence on the North Anatolian fault under the Marmara Sea

Tohid NOZADKHALIL[1],* , **Ziyadin ÇAKIR[1]** , **Semih ERGİNTAV[2]**, **Uğur DOĞAN[3]**, **Thomas R. WALTER[4]**

[1]Department of Geological Engineering, Faculty of Mines, İstanbul Technical University, İstanbul, Turkiye
[2]Geodesy, Kandilli Observatory and Earthquake Research Institute, Boğaziçi University, İstanbul, Turkiye
[3]Geomatic Engineering, Faculty of Civil Engineering, Yıldız Technical University, İstanbul, Turkiye
[4]Geophysics, Helmholtz Centre Potsdam-GFZ, Potsdam, Germany

Abstract: We map surface deformation in the Thrace region of Turkey using the Sentinel-1 Synthetic Aperture Radar (SAR) data. Interferometric Synthetic Aperture Radar (InSAR) time series analysis of the SAR data acquired between 2014 and 2020 on ascending and descending orbits reveals large-scale subsidence (~110 × 60 km) with rates reaching up to 10 ± 1.5 mm/yr. We relate this deformation to natural gas reservoir operations, such as gas exploitation and extraction activities that have been taking place in the region for decades, an inference being supported by the strong correlation between the InSAR time series and the variation in natural gas production during the same time period in the Thrace region reported by the Energy Market Regulation Authority of Turkey. Assuming that the observed subsidence is caused by compaction of sediments in the natural gas reservoirs, we construct a triangulated surface enveloping roughly at the bottom of the gas extraction wells and use it to invert the amount of negative opening (hence volume loss) on triangular elements that are assumed to be buried in an elastic and homogeneous medium. Coulomb stress changes caused by this volume change on the North Anatolian Fault at the Sea of Marmara are found to be insignificant (less than 10^{-5} Mega-Pascal) to perturb the state of the stress around the Marmara seismic gap. Yet, the large-scale subsidence revealed in this study needs to be taken into consideration when assessing hazards for the infrastructures, settlements, and other engineering structures, particularly in case of a large earthquake in the Marmara Seismic Gap.

Key words: InSAR, subsidence, Coulomb stress, Marmara fault, compound dislocation model, Poly3D

1. Introduction

Subsidence and induced seismicity due to excessive groundwater pumping, geothermal operations, and the development of hydrocarbon extraction methods have recently attracted considerable attention all over the world. Following the free access policy of the European Commission for the Sentinel-1 SAR data available since 2014, InSAR has been extensively used to study these phenomena. Subsidence can also be triggered by groundwater extraction both in agricultural and residential areas resulting in infrastructure and building damages. Subsidence in various cities such as; Tehran and Yazd in Iran; Mexico City in Mexico; Bursa and Konya in Turkey; and Taiyuan basin in North China has been revealed using InSAR (Castellazzi et al., 2016; Aslan et al., 2020; Haghshenas Haghighi & Motagh, 2021; Motagh et al., 2007; Şireci et al., 2021; Tang et al., 2022). InSAR investigation on geothermal fields in western Anatolia reveals local pressure drops in the fields and significant subsidence

on the Earth's surface, implying the importance of the systematic monitoring and identification of deformation patterns in spatial-temporal extent as well as providing an essential data source for reservoir characterization and field development planning (Aslan et al., 2022).

Furthermore, fluid injection for shale gas hydraulic fracturing can increase the pressure and induce earthquakes. Stress redistribution and pore pressure changes within and surrounding the reservoir may lead to geomechanical changes, fault reactivation, micro-seismicity, and even damaging earthquakes (Ellsworth, 2013; Giammanco et al., 2008; Yamashita & Suzuki, 2009). Revision of the locations of 6 events with magnitudes 4.0 ≤ ML ≤ 5.1 between 1938 and 1944 in the California Basin reveals induced seismicity caused by stress and strain changes associated with oil production. (Hough & Bilham, 2018a, 2018b). Both Mw 5.8 in September 2016 near Pawnee, Oklahoma, United States (Yeck et al., 2017) and Mw 4.7 in January 2017 in the Sichuan Basin, China

* Correspondence: nozadkhalil18@itu.edu.tr

421

(Lei et al., 2017) events are injection induced earthquakes. Spatial and temporal variation of Coulomb Failure Stress in western Oklahoma is dominated by changes in poroelastic stresses and pore pressure, as a result of fluid injection (Zhai et al., 2019). Induced earthquakes could be controlled by groundwater extraction that correlates with slip distribution similar to the Eastern Betics Shear Zone in south-eastern Spain (González et al., 2012).

Any earth's surface and subsurface activity that affects the stress field in its vicinity significantly may trigger or accelerate potential future hazardous events particularly in regions with high seismic risk. During the 20th century, westward propagation of M > 7 failures (Ambraseys, 1970; Barka, 1966; Stein et al., 1997) along the North Anatolian Fault (NAF) ended at İzmit in 1999. Due to the 1912 Şarköy and the 1999 İzmit earthquake (Figure 1) to the west and east, respectively, the Central Marmara Fault (CMF) is designated as a seismic gap. Coulomb stress change, resulted from the 1999 İzmit event to the west of this seismic gap, brought forward the next earthquake in the Sea of Marmara by 12 years (Çakır et al., 2003). In addition, GPS observations reveal 10–15 mm/yr of slip

rate for the Princes' Islands Fault (PIF) with no evidence of strain accumulation for the CMF (Ergintav et al., 2014). İstanbul, with a population of over 15 million people and a primarily financial and industrial centre of Turkey, is critical for earthquake and ground motion risks related with faulting, landslides, and sediment compaction processes.

In this study, we use the advanced InSAR technique to map the surface motions in the eastern Thrace basin (NW Turkey) where natural gas reservoir processes and extraction have been carried out with tens of wells for decades from various formations at different depths (Figure 1). We also model the mean InSAR velocity maps using elastic dislocations and calculate the Coulomb stress variation on CMF caused by volume loss due to natural gas extraction.

2. Thrace basin

2.1. Geology
Thrace Basin is bounded by the Triassic to Jurassic metamorphic rocks of the Strandja massif in the north and the Biga Peninsula in the south. This large triangular-
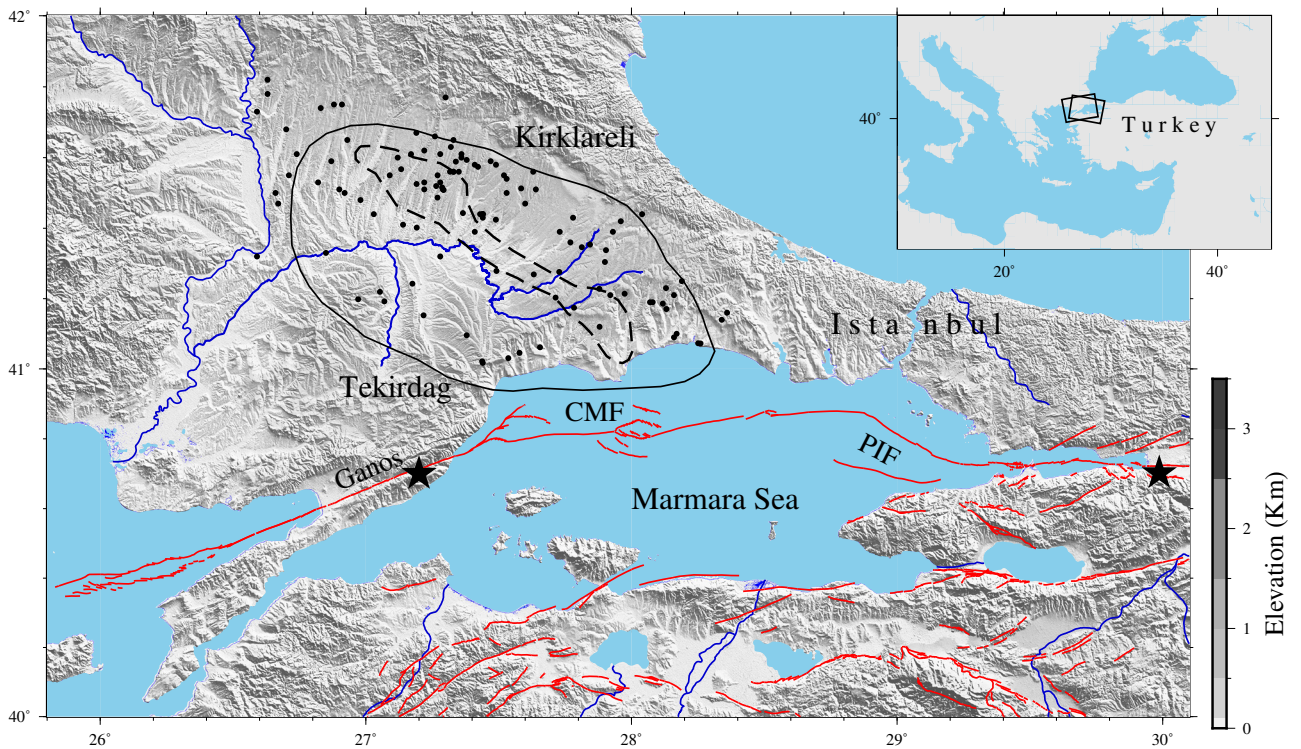
Figure 1. Topographic and tectonic map of the Thrace basin and Marmara Sea region in northwestern Turkey. Black boxes in the inset map show the frames of the T131 (ascending) and T036 (descending) orbits of the Sentinel TOPSAR images. Red and blue solid-lines display active faults (after Emre et al. 2013) and permanent rivers, respectively. Black stars display the location of the 1912 Şarköy event on Ganos Fault and at the west of Cental Marmara Fault (CMF) and the 1999 İzmit event east of Princes' Islands Fault (PIF), respectively. Black solid circles are the available location of active and inactive natural gas production facilities (after Gürgey et al. 2005; Yılmaz et al. 2016). Black solid and dashed lines display the geographic extent of Hamitabat formation and the area that is active after Gürgey (2009), respectively.

shaped Tertiary depression is filled with more than 8–9 km of an upward shallowing sequence of Mid-Eocene to Oligocene clastic strata (Gürgey, 2009). The metamorphic basement of the Thrace basin is mostly covered by a combination of deep marine turbidite, sandstone, silt, and shale deposits known as Hamitabat formations with an angular unconformity. This reveals a rapid subsidence of metamorphic and crystalline basement at the Middle Eocene. The Hamitabad formation is the main natural gas reservoir in the Thrace basin (Figure 2) and is overlain by the Soğucak Formation, a thin layer of shallow-marine limestones which pass up into shales, marls, and turbiditic sandstones of the upper Eocene to lower Oligocene Ceylan Formation. With the regression of sea level in the Late Oligocene, deltaic deposition began with prodelta facies of tuffy shales and marls; the Mezardere formation, delta front facies deposition characterised by coarsening upward sandy sediments; the Osmancık Formation, and delta plain sediments; the Danişmen Formation. This deltaic Oligocene sequence, which forms reservoirs for natural gas, is unconformably covered by the Mio–Pliocene fluvio-lacustrine deposits of Ergene formation (Gürgey, 2009; OKAY et al., 2010; Okay & Topuz, 2017; Turgut et al., 1991).

2.2. Gas production activities

The Thrace Basin is bounded by the Triassic to Jurassic metamorphic rocks of the Strandja massif to the north and the Biga Peninsula to the south. This extensive Tertiary depression is filled (Figure 1) with more than 8–9 km of an upward shallowing sequence of Mid-Eocene to Oligocene clastic strata. Explorations, which started in the early 1960s, led to the discovery of various gas fields ranging in size between 3 and 50 million m^3 in this basin (Gürgey, 2009). Hoşgörmez et al. (2005) report that the gas accumulations have different origins based on molecular and isotopic composition of gases. Gas production is feasible in a variety of formations at different depths, including the Eocene Hamitabat formation, Upper Eocene–Lower Oligocene Ceylan, and formation and the Oligocene Mezardere in the Thrace basin. According to annual reports of the Energy Market Regulation Authority (EPDK) from 2014 to 2020, more than 60% of natural gas production in Turkey was carried out in the Thrace basin including Tekirdağ and Kırklareli provinces (Turkish Natural Gas Market Reports, 2020). The report discloses that gas produced from Thrace basin is ~1870 million Standard cubic meters (Sm^3). Natural gas production in 2014 was ~350 million Sm^3 which decreased to ~ 217 million Sm^3 in 2018 and increased to ~260 million Sm^3 in 2020.

3. Mapping surface deformation using InSAR

To map the surface deformation in the Trace basin, we use the Persistent Scatterer InSAR (PSI) technique, an advanced InSAR technique that can detect subtle motions on the earth's surface associated with various geological processes or anthropogenic activities. This multitemporal InSAR method identifies discrete and stable temporal phase scatterers from InSAR images stack even with baselines larger than critical baseline (Ferretti et al., 2000, 2001; Hooper et al., 2012).

We process the C-band (~5.8 cm wavelength) TOPSAR dataset of the Sentinel-1 satellites between 2014 and 2020. Interferograms are generated with the GMTSAR software, an open-source (GNU General Public Licence) InSAR processing tool designed for users of Generic Mapping Tools (GMT) (Sandwell et al., 2011). More than 800 Interferograms on both ascending (T131) and descending (T36) orbits are used for time series calculations. Time-series of interferograms are obtained using the StaMPS (Stanford Method for Persistent Scatterers) multitemporal InSAR software (Hooper, 2008; Hooper et al., 2004). We also use a power law correction method of Toolbox for Reducing Atmospheric InSAR Noise (TRAIN) to reduce tropospheric signals locally (Bekaert et al., 2015).

Mean line of sight (LOS) velocity maps obtained in both ascending and descending orbits are shown in Figures 2a and 2b. While warm colours (red) indicate motion away from the satellite (subsidence and/or eastward motion for the ascending and westward motion for the descending in horizontal direction), cold colours (blue) indicate motion towards the satellite (uplift and/or eastward motion for the descending and westward motion for the ascending in horizontal direction). In the Thrace basin, the two velocity fields are in good agreement and show motion away from satellites (red colours) in both orbits, implying that the motion is mostly subsidence. Located 30 to 60 km to the north of the NAF in the Sea of Marmara, the subsidence in the Thrace basin has an elongated elliptical pattern and covers an area of ~60 km wide and 110 km long (~5500 km^2).

Considering that both orbits measure the projection of a real deformation vector on the LOS, we decompose the LOS measurements into vertical and horizontal (east-west) components (Samieie-Esfahany et al., 2009) (Figures 2c and 2d). The projected profile on vertical and horizontal velocity fields along the long and short (A-A` and B-B` in Figure 2c, respectively) axis of the elliptical deformation show that subsidence reaches locally to 10 ± 1.5 mm/yr (Figures 3a and 3b).

Time series analysis (Figure 3a) shows that subsidence increases with an almost linear rate until 2018 and variates between 2018 and 2020 and show a very strong correlation with changes in the production rate with a delay in time. This time lag between the time series of surface deformation and gas production in Tekirdağ and Kırklareli reported by EPDK is corrected by a 3 month shift in the production time series.
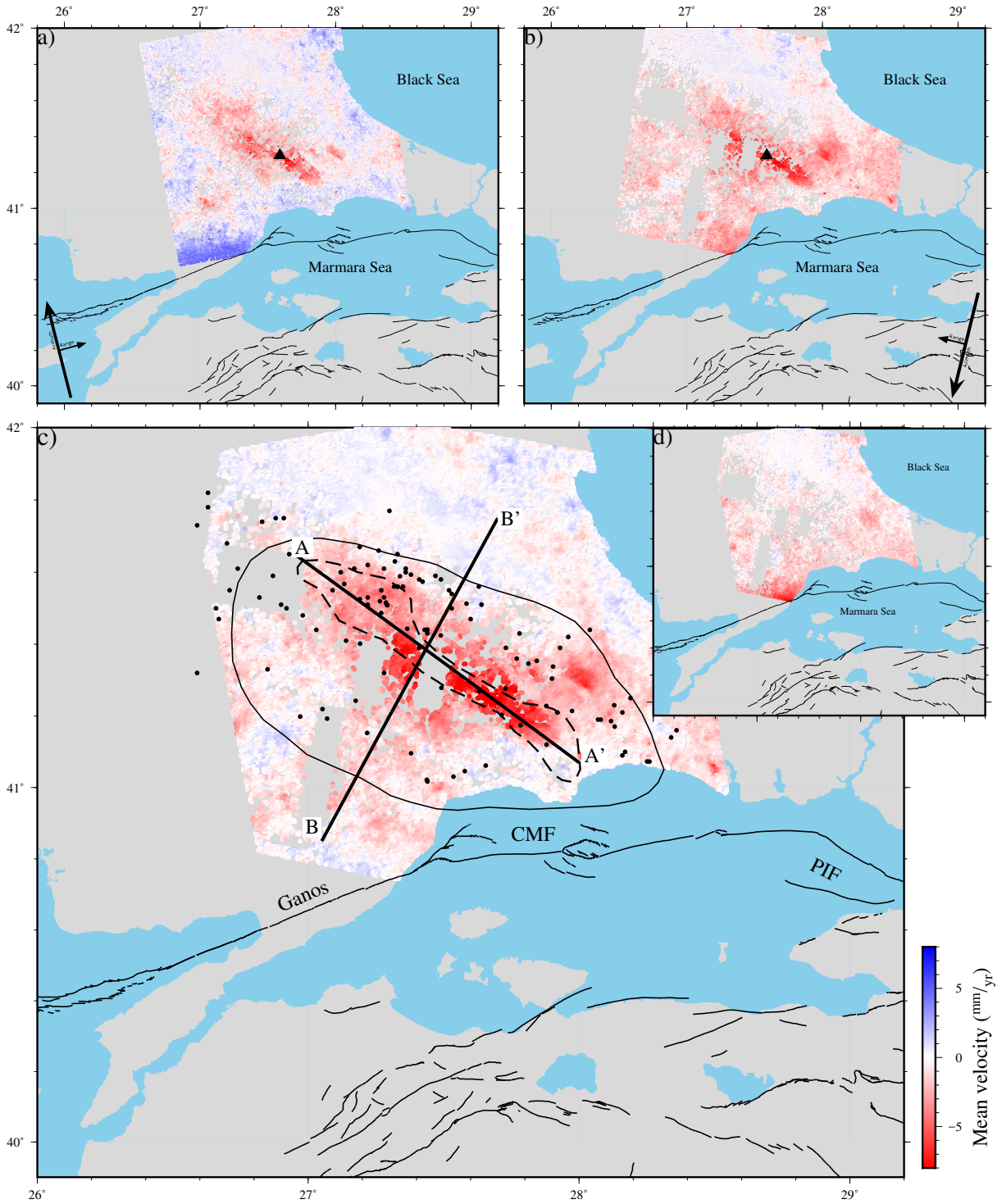
Figure 2. Mean LOS velocity fields of ascending (a) and descending (b) orbits in the Thrace basin from Sentinel TOPSAR data acquired between 2014 and 2020. Mean LOS velocity fields are cropped to isolate the subsidence in the Trace basin. Warm (red) and cold (blue) colours show motion away from and toward the satellite, respectively. Therefore, the presence of the red colour in both orbits indicates the existence of subsidence in the Thrace region. Subsiding area is bounded in the area with high density of active natural gas fields signified by black solid circles (modified after Gürgey et al. 2005; Yılmaz et al. 2016). In addition, the subsidence pattern correlates well with region where natural gas has been currently exploited (dashed black line) within the Hamitabat formation (solid black line) mentioned in Gürgey (2009). Vertical and horizontal deformation rates along the profiles A-A` and B-B` are shown in Figures 3a and 3b and black triangle on LOS map (a and b) displays the location of persistent scatterers used for the time-series plot in Figure 3c.
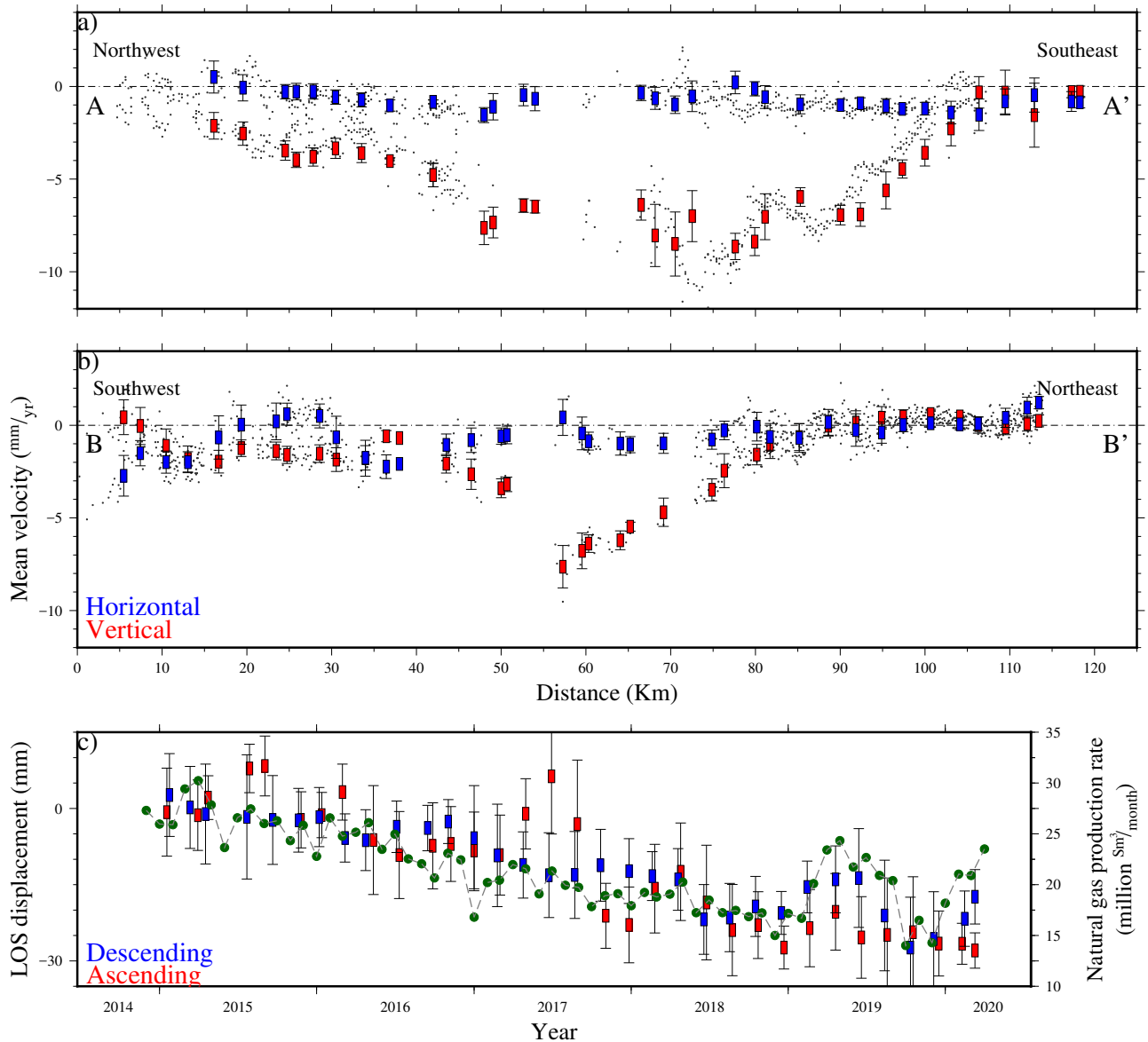
Figure 3. Projection of vertical (red bars) and horizontal (east-west) (blue bars) mean velocities along the profiles A-A` (a) and B-B` (b) in Figure 2c. Both profiles expose up to 10 ± 1.5 mm/yr of deformation rate in Thrace region. Time series (c) of persistent scatterers (black star in Figure 2a and 2b) from both ascending (blue bars) and descending (red bars) orbits. Monthly reports of the Energy Market Regulation Authority (EPDK) in the Tekirdağ and Kırklareli from 2014 to 2020 (dark-green solid circles) disclose a constant annual decrease during 2014–2018 years with few seasonal variations and a sharp increase and decrease in production rate in 2019 and again an increase in 2020.
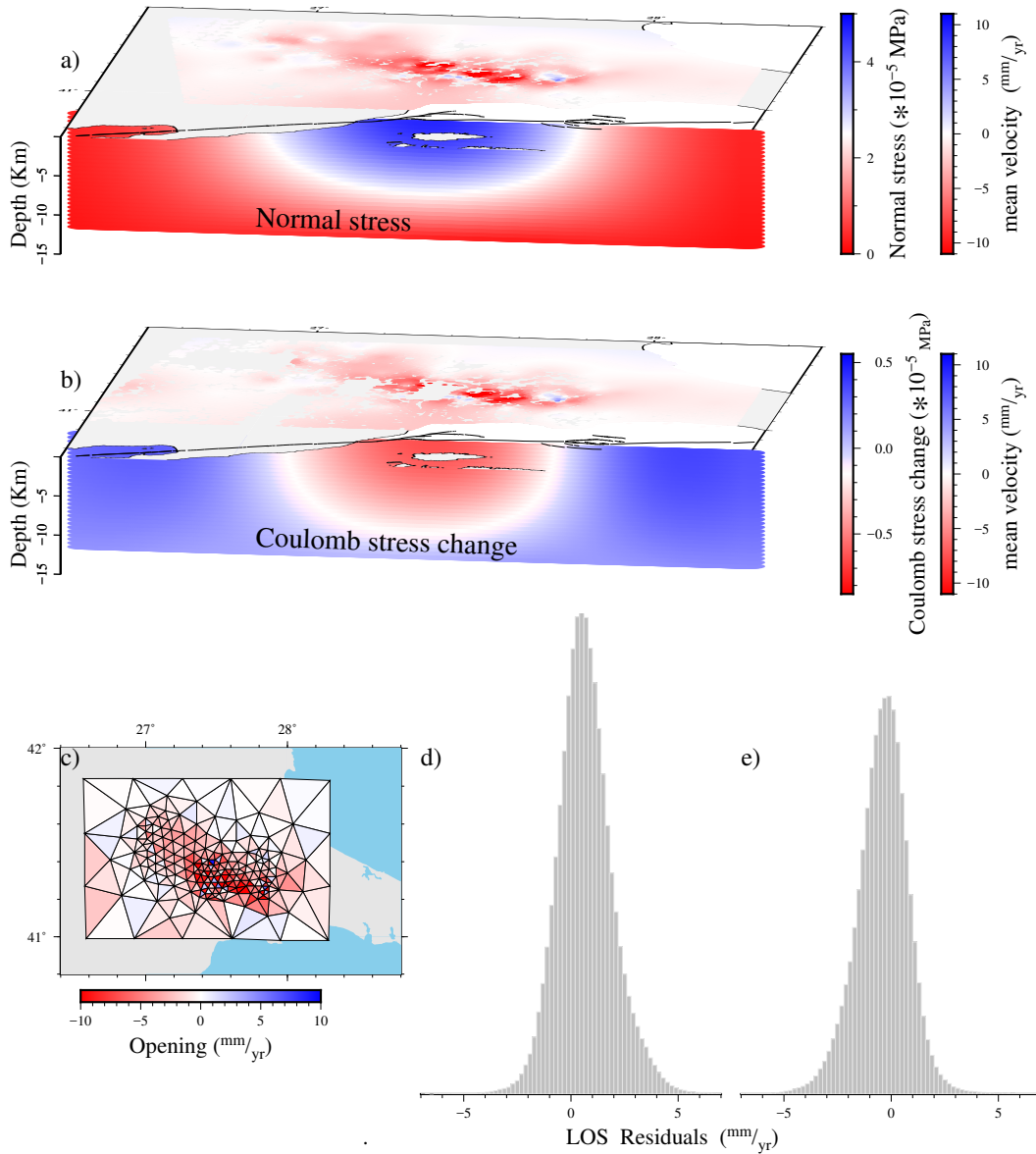
In addition to the subsidence in the Thrace basin, plate motions across the Sea of Marmara and the Ganos Fault on land are also clearly revealed by the PSI method (Figure 4). While the southern block of the CMF moves towards the satellite in the ascending orbit (Figure 4a), it moves away from the satellite in the descending orbit (Figure 4b), indicating the right-lateral sense of motion between the Eurasian and Anatolian plates. Strain accumulation across the Ganos Fault is also clearly revealed by the PSI results.

4. Dislocation model

Assuming that the observed subsidence is due to the compaction of sediments as a result of natural gas extraction, we model the mean LOS velocity field using volume loss in elastic and homogeneous half-space. We constructed a triangulated surface at a depth of 2 km that is the average depth of extraction wells (Gürgey et al., 2005; Yilmaz et al., 2016) in the study area (unfortunately, information about the depths of most wells is not available). Volume
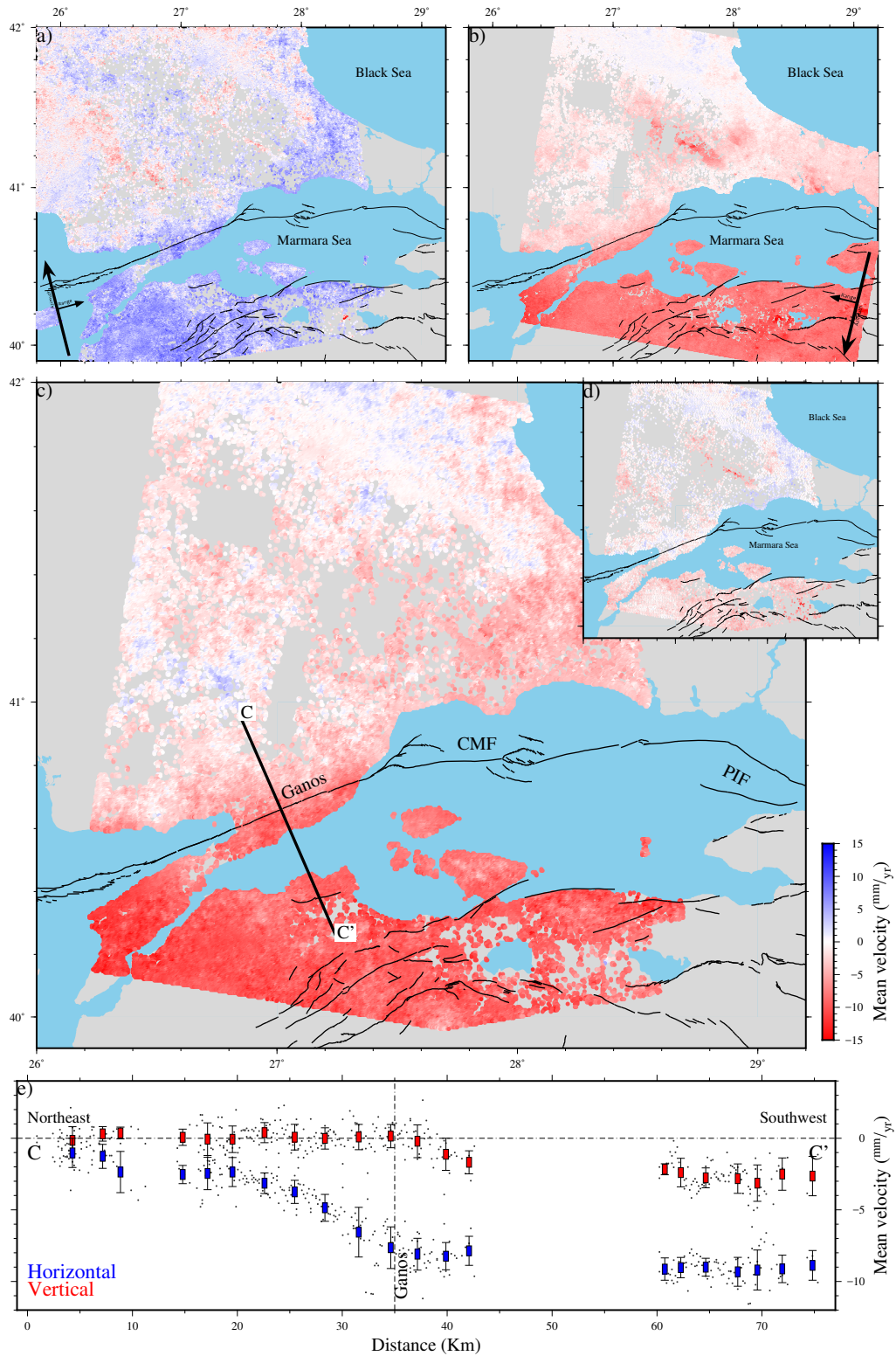
Figure 4. Mean LOS velocity fields on ascending (a) descending (b) orbits extended to the south with regard to representing deformations related to plate motions across the Sea of Marmara and the Ganos Fault. Both the LOS (a, b) and decomposed east-west horizontal (c) velocity fields reveal clearly the interseismic strain accumulation across the Ganos fault. Vertical velocity field (d) does not show any clear differential motion across the Ganos fault. Projection of horizontal (blue bars) and vertical (red bars) velocities along the C-C` profile (c) illustrate ~10 ± 2 mm/yr of right lateral deformation with normal motions less than 3 mm/yr along the Ganos Fault.

Figure 5. Normal stress (a) and Coulomb stress change (b) on the CMF due to subsidence in the Thrace basin and modelled mean LOS velocity. The volume loss due to compaction in sediments leads to a decrease in Coulomb stress along the CMF in the Tekirdağ basin because of the increased normal stress on it. (c) Poly3d model of surface deformation. Residuals between the model and ascending and descending InSAR data are shown in d and 3, respectively. (e) and (d) are residual histograms for Ascending and Descending, respectively.

loss in sediments is modeled with a negative opening on triangular elements using the Poly3dinv inversion software, a three-dimensional slip-inversion method on triangular elements (Maerten, 2005). This method is based on the analytical solution for an angular dislocation in a linear-elastic, homogeneous, isotropic, half-space. Poly3dinv employs the Poly3D (Thomas, 1993) that uses a set of planar triangular elements of constant displacement discontinuity to model deformation surfaces. The model

estimates ~15.5 ± 0.1 million m³/yr of volume loss rate in sediments as a result of subsidence in the Thrace basin.

5. Coulomb stress model
We calculate Coulomb stress changes to determine the influence of subsidence caused by gas extraction on the state of stress on the NAF in the Marmara Sea. To avoid numerical artifacts and structural imperfections, we employed the compound dislocation model (CDM)

which is an artifact-free solution to calculate stress field and deformation associated with rectangular dislocations with full rotational degrees of freedom in an elastic full-space and half-space (Nikkhoo et al., 2017). For this purpose, we gridded triangular elements using flexible tension continuous curvature splines (Smith & Wessel, 1990) and divided them into small rectangular cells, and assume that they are point sources (Nikkhoo et al., 2017). The point CDM (pCDM) is dimensionless and represents volumetric changes due to expansion or contraction in all directions in space. We calculate the pCDM from the potency and aspect ratios regardless of the shape of the deformation sources. The potency is the product of area and slip (opening value in tensile) (Aki & Richard, 2002). The product of opening by area is equal to the potency of point sources in the horizontal plane.

We calculate normal stress, shear stress, and Coulomb stress changes on a smooth and continuous vertical surface that coincides roughly with the CMF from the surface to 15 km of depth. Figures 5a, 5b, and 5c show the variation of normal stress and Coulomb stress changes along the CMF due to the modelled compaction in the gas reservoir. The modeled surface deformation mimics well the InSAR observations due to the proximity of modelled plane to the surface and small sizes of triangular elements where deformation gradient is high (Figures 5d and 5e).

As can be seen, the volume loss due to compaction in sediments leads to a decrease in Coulomb stress along the CMF in the Tekirdağ basin because of the increased normal stress on it. Coulomb stress on the fault increases towards both edges of the Tekirdağ basin, promoting failure on the fault. However, Coulomb stress changes are on the order of 10^{-5} Mega-Pascal, hence too small to affect the state of stress on the CMF.

6. Discussions and conclusions

Mapping surface motions using PS-InSAR for both ascending and descending orbits reveals widespread subsidence with an elongated elliptical pattern in the Thrace basin, northwestern Turkey. Decomposition of mean LOS velocities to vertical and horizontal components indicates a maximum of 10 ± 1.5 mm/yr of subsidence. This gives rise to a total deformation up to 50 ± 10 mm between 2014–2020. The observed subsidence may partially be resulted from excessive groundwater extraction. However, because of (1) the subsiding region being located within an active natural gas field, and (2) the similarities between spatial pattern of subsidence and the Hamitabat formation (Figure 2c) from which gas extraction has been carried out (Gürgey, 2009) suggest that this vertical motion occurs most probably due to the natural gas extraction. This is also supported by the strong correlation between the gas production rate and InSAR time series (Figure 3c).

Assuming that the observed subsidence results mainly from volume loss due to sediment compaction, we model the surface deformation using negative opening on triangular elements in an elastic half space. Using such this model we evaluate ~15.5 ± 0.1 million m^3/yr volume loss in sediments as the result of subsidence in the Thrace basin. We then calculate Coulomb stress changes on the Central Marmara Fault segment of the North Anatolian Fault. The Coulomb Stress variation on CMF due to subsidence is found to be negligible as it is on the order of 10^{-5} Mega-Pascal. However, the effect of this subsidence on industrial and residential buildings and infrastructure cannot be ignored for long time periods.

Catalogues of Kandilli Observatory and AFAD do not show much seismic activity associated with natural gas production, which is most probably due to the poor instrumental coverage in the region.

Furthermore, InSAR results reveal a clear signal of interseismic strain accumulation along the Ganos fault and ~10 ± 2 mm/yr dextral sense of motion between the Eurasian and Anatolian plates. Analysis of InSAR data shows that the present-day kinematics of western Anatolia has no significant effects on the Thrace basin.

References

Aki K, Richard PG (2002). Quantitative Seismology. 2nd Edition.

Ambraseys NN (1970). Some characteristic features of the Anatolian fault zone. Tectonophysics 9 (2–3): 143–165. https://doi.org/10.1016/0040-1951(70)90014-4

Aslan G, Aydin H, Çakir Z (2022). Wide-area ground deformation monitoring in geothermal fields in western Turkey. Turkish Journal of Earth Sciences 31 (3): 247–259. https://doi.org/10.55730/1300-0985.1771

Aslan G, Foumelis M, Raucoules D, De Michele M, Bernardie S et al. (2020). Landslide Mapping and Monitoring Using Persistent Scatterer Interferometry (PSI) Technique in the French Alps. Remote Sensing 12 (8): 1305. https://doi.org/10.3390/rs12081305

Barka A (1966). Slip distribution along the North Anatolian fault associated with the large earthquakes of the period 1939 to 1967. Bulletin of the Seismological Society of America 86 (5): 1238–1254.

Bekaert DPS, Hooper A, Wright TJ (2015). A spatially variable power law tropospheric correction technique for InSAR data. Journal of Geophysical Research: Solid Earth 120 (2): 1345–1356. https://doi.org/10.1002/2014JB011558

Çakır Z, Barka AA, Evren E (2003). Coulomb Stress Interactions and the 1999 Marmara Earthquakes. Turkish Journal of Earth Sciences 12: 91–103.

Castellazzi P, Arroyo-Domínguez N, Martel R, Calderhead AI, Normand JCL et al. (2016). Land subsidence in major cities of Central Mexico: Interpreting InSAR-derived land subsidence mapping with hydrogeological data. International Journal of Applied Earth Observation and Geoinformation 47: 102–111. https://doi.org/10.1016/j.jag.2015.12.002

Ellsworth WL (2013). Injection-Induced Earthquakes. Science 341 (6142). https://doi.org/10.1126/science.1225942

Ergintav S, Reilinger RE, Çakmak R, Floyd M, Çakır Z et al. (2014). Istanbul's earthquake hot spots: Geodetic constraints on strain accumulation along faults in the Marmara seismic gap. Geophysical Research Letters 41 (16): 5783–5788. https://doi.org/10.1002/2014GL060985

Ferretti A, Prati C, Rocca F (2000). Nonlinear subsidence rate estimation using permanent scatterers in differential SAR interferometry. IEEE Transactions on Geoscience and Remote Sensing 38 (5): 2202–2212. https://doi.org/10.1109/36.868878

Ferretti A, Prati C, Rocca F (2001). Permanent scatterers in SAR interferometry. IEEE Transactions on Geoscience and Remote Sensing 39 (1): 8–20. https://doi.org/10.1109/36.898661

Giammanco S, Palano M, Scaltrito A, Scarfì L, Sortino F (2008). Possible role of fluid overpressure in the generation of earthquake swarms in active tectonic areas: The case of the Peloritani Mts. (Sicily, Italy). Journal of Volcanology and Geothermal Research 178 (4): 795–806. https://doi.org/10.1016/j.jvolgeores.2008.09.005

González P J, Tiampo KF, Palano M, Cannavó F, Fernández J (2012). The 2011 Lorca earthquake slip distribution controlled by groundwater crustal unloading. Nature Geoscience 5 (11): 821–825. https://doi.org/10.1038/ngeo1610

Gürgey K (2009). Geochemical overview and undiscovered gas resources generated from Hamitabat petroleum system in the Thrace Basin, Turkey. Marine and Petroleum Geology 26 (7): 1240–1254. https://doi.org/10.1016/j.marpetgeo.2008.08.007

Gürgey K, Philp RP, Clayton C, Emiroğlu H, Siyako M (2005). Geochemical and isotopic approach to maturity/source/mixing estimations for natural gas and associated condensates in the Thrace Basin, NW Turkey. Applied Geochemistry 20 (11): 2017–2037. https://doi.org/10.1016/j.apgeochem.2005.07.012

Haghshenas Haghighi M, Motagh M (2021). Land subsidence hazard in iran revealed by country-scale analysis of sentinel-1 insar. The International Archives of the Photogrammetry, Remote Sensing and Spatial Information Sciences XLIII-B3-2021: 155–161. https://doi.org/10.5194/isprs-archives-XLIII-B3-2021-155-2021

Hooper A (2008). A multi-temporal InSAR method incorporating both persistent scatterer and small baseline approaches. Geophysical Research Letters 35 (16): L16302. https://doi.org/10.1029/2008GL034654

Hooper A, Bekaert D, Spaans K, Arıkan M (2012). Recent advances in SAR interferometry time series analysis for measuring crustal deformation. Tectonophysics 1 (13): 514–517. https://doi.org/10.1016/j.tecto.2011.10.013

Hooper A, Zebker H, Segall P, Kampes B (2004). A new method for measuring deformation on volcanoes and other natural terrains using InSAR persistent scatterers. Geophysical Research Letters 31 (23): https://doi.org/10.1029/2004GL021737

Hoşgörmez H, Yalçın MN, Cramer B, Gerling P, Mann U (2005). Molecular and isotopic composition of gas occurrences in the Thrace basin (Turkey): origin of the gases and characteristics of possible source rocks. Chemical Geology 214 (1–2): 179–191. https://doi.org/10.1016/j.chemgeo.2004.09.004

Hough SE, Bilham R (2018a). Poroelastic stress changes associated with primary oil production in the Los Angeles Basin, California. The Leading Edge 37 (2): 108–116. https://doi.org/10.1190/tle37020108.1

Hough SE, Bilham R (2018b). Revisiting Earthquakes in the Los Angeles, California, Basin During the Early Instrumental Period: Evidence for an Association With Oil Production. Journal of Geophysical Research: Solid Earth 123 (12): 10,684-10,705. https://doi.org/10.1029/2017JB014616

Lei X, Huang D, Su J, Jiang G, Wang X et al. (2017). Fault reactivation and earthquakes with magnitudes of up to Mw4.7 induced by shale-gas hydraulic fracturing in Sichuan Basin, China. Scientific Reports 7 (1): 7971. https://doi.org/10.1038/s41598-017-08557-y

Maerten F (2005). Inverting for Slip on Three-Dimensional Fault Surfaces Using Angular Dislocations. Bulletin of the Seismological Society of America 95 (5): 1654–1665. https://doi.org/10.1785/0120030181

Motagh M, Hoffmann J, Kampes B, Baes M, Zschau J (2007). Strain accumulation across the Gazikoy-Saros segment of the North Anatolian Fault inferred from Persistent Scatterer Interferometry and GPS measurements. Earth and Planetary Science Letters 255 (3–4): 432–444. https://doi.org/10.1016/j.epsl.2007.01.003

Nikkhoo M, Walter TR, Lundgren PR, Prats-Iraola P (2017). Compound dislocation models (CDMs) for volcano deformation analyses. Geophysical Journal International 208 (2): 877–894. https://doi.org/10.1093/gji/ggw427

Okay AI, Özcan E, Cavazza W, Okay N, Less G (2010). Basement Types, Lower Eocene Series, Upper Eocene Olistostromes and the Initiation of the Southern Thrace Basin, NW Turkey. Turkish Journal of Earth Sciences 19 (1): 1-25. https://doi.org/10.3906/yer-0902-10

Okay AI, Topuz G (2017). Variscan orogeny in the Black Sea region. International Journal of Earth Sciences 106 (2): 569–592. https://doi.org/10.1007/s00531-016-1395-z

Samieie-Esfahany S, Hanssen RF, Thienen-Visse KV, Muntendam-Bos AG (2009, September). On the effect of horizontal deformation on InSAR subsidence estimates.

Sandwell D, Mellors R, Tong X, Wei M, Wessel P (2011). Open radar interferometry software for mapping surface Deformation. Eos, Transactions American Geophysical Union 92 (28): 234–234. https://doi.org/10.1029/2011EO280002

Şireci N, Aslan G, Çakir Z (2021). Long-term spatiotemporal evolution of land subsidence in Konya metropolitan area (Turkey) based on multisensor SAR data. Turkish Journal Of Earth Sciences 30 (5): 681–697. https://doi.org/10.3906/yer-2104-22

Smith WHF, Wessel P (1990). Gridding with continuous curvature splines in tension. GEOPHYSICS 55 (3): 293–305. https://doi.org/10.1190/1.1442837

Stein RS, Barka AA, Dieterich JH (1997). Progressive failure on the North Anatolian fault since 1939 by earthquake stress triggering. Geophysical Journal International 128 (3): 594–604. https://doi.org/10.1111/j.1365-246X.1997.tb05321.x

Tang W, Zhao X, Motagh M, Bi G, Li J et al. (2022). Land subsidence and rebound in the Taiyuan basin, northern China, in the context of inter-basin water transfer and groundwater management. Remote Sensing of Environment 269: 112792. https://doi.org/10.1016/j.rse.2021.112792

Thomas AL (1993). Poly3D: A Three-Dimensional, Polygonal Element, Displacement Discontinuity Boundary Element Computer Program with Applications to Fractures, Faults, and Cavities in the Earth's Crust. MSc, Stanford University, California, US.

Turgut S, Türkaslan M, Perinçek D (1991). Evolution of the Thrace sedimentary basin and its hydrocarbon prospectivity. In: Spencer AM (ed) Generation, accumulation, and production of Europe's hydrocarbons. Generation, Accumulation, and Production of Europe's Hydrocarbons, 415–437.

Turkish Natural Gas Market Reports. (2020). EPDK (Republic of Turkey Energy Market Regulatory Authority Strategyc). https://www.epdk.gov.tr/Detay/Icerik/1-1275/natural-gasreports

Yamashita T, Suzuki T (2009). Quasi-static fault slip on an interface between poroelastic media with different hydraulic diffusivity: A generation mechanism of afterslip. Journal of Geophysical Research 114 (B3): B03405. https://doi.org/10.1029/2008JB005930

Yeck WL, Hayes GP, McNamara DE, Rubinstein JL, Barnhart WD, Earle PS, Benz HM (2017). Oklahoma experiences largest earthquake during ongoing regional wastewater injection hazard mitigation efforts. Geophysical Research Letters 44 (2): 711–717. https://doi.org/10.1002/2016GL071685

Yilmaz K, Umul B, Davis J, Nilson G (2016). Tight gas development in the Mezardere Formation, Thrace Basin Turkey. Journal of Natural Gas Science and Engineering 33: 551–561. https://doi.org/10.1016/j.jngse.2016.05.049

Zhai G, Shirzaei M, Manga M, Chen X (2019). Pore-pressure diffusion, enhanced by poroelastic stresses, controls induced seismicity in Oklahoma. Proceedings of the National Academy of Sciences 116 (33): 16228–16233. https://doi.org/10.1073/pnas.1819225116